

# Degradation Identification and Prognostics of Proton Exchange Membrane Fuel Cell Under Dynamic Load

Meiling Yue<sup>a,1</sup>, Zhongliang Li<sup>b</sup>, Robin Roche<sup>c</sup>, Samir Jemei<sup>a</sup>, Nouredine Zerhouni<sup>d</sup>

<sup>a</sup>FEMTO-ST Institute, FCLAB, Univ. Bourgogne Franche-Comté, CNRS, Belfort, France

<sup>b</sup>LIS Laboratory, Aix-Marseille University, CNRS, Marseille, France

<sup>c</sup>FEMTO-ST Institute, FCLAB, Univ. Bourgogne Franche-Comté, UTBM, CNRS, Belfort, France

<sup>d</sup>FEMTO-ST Institute, FCLAB, Univ. Bourgogne Franche-Comté, ENSMM, CNRS, Belfort, France

## Abstract

Proton exchange membrane (PEM) fuel cell has seen its recent increasing deployment in both automotive and stationary applications. However, the unsatisfied durability of the fuel cell has barred in the way of its successful commercialization. Recent research on prognostics and predictive maintenance has demonstrated its effectiveness in predicting the system failure and improving the durability of the PEM fuel cell. This paper contributes to developing a degradation identification method for the PEM fuel cell operating under dynamic load. A degradation indicator is proposed based on the polarization model and the nonlinear regression method is applied to extract the degradation feature by segmenting the voltage measurement. To perform prognostics, a machine learning method based on a multi-step echo state network is developed, in which a sliding window is used to recursively reformulate the input sequence with predicted values in the prediction phase. The length of the sliding window is optimized by a genetic algorithm. The proposed method is verified on the experimental PEM fuel cell degradation data and improves the prediction performance on both accuracy and computation speed when comparing with other prognostics methods.

## Keywords:

dynamic load, echo state network, PEM fuel cell, health indicator, prognostics

## 1. Introduction

Although fossil fuels still account for the majority of global energy demand, an energy transition is taking place. Hydrogen, as one of the cleanest fuels, has driven increasing attention around the world, which is regarded as a potential solution to today's environmental problems and resource exhaustion. ~~Using hydrogen as the fuel, To make use of hydrogen, fuel cell re-electrification is a preferable way to maximize its potential benefits, as fuel cells can convert the chemical energy of the hydrogen into electrical energy directly with an efficiency up to 60 to 80%, while the by-product is only water.~~ Among different types of fuel cells, proton exchange membrane (PEM) fuel cells, which take advantages of their fast start-up characteristics and low operating temperatures, are now commercially applied in a variety of stationary and embedded applications [1].

On the road to the massive commercialization of PEM fuel cells, enhancing their durability is a prior challenge. The currently achieved durability of PEM fuel cells in automotive applications is around 4000 - 5000 hours, while an 8000-hour lifetime is the ultimate goal [2]. Efforts have been made to investigate PEM fuel cell degradation mechanisms, especially for those operating under dynamic load [3, 4]. For example, dynamic vehicle cycles in rated and idling conditions are simulated in [5], in which the PEM fuel cell is subjected to different degradation mechanisms causing varying stack voltage

degradation rate. An accelerated degradation test is conducted in [6] with normal vehicle driving cycles where significant degradation of the fuel cell has been observed. Varying thermal/humidity state, changing reactant demand and **potential voltage** cycling are identified as the principal reasons for PEM fuel cell degradation in dynamic operating conditions [7].

Fuel cell performance loss can be easily observed by evaluating the stack voltage degradation and under constant operating conditions, it is measured directly. Various works on PEM fuel cell degradation estimation and prognostics have been conducted using the stack voltage as the direct health indicator [8, 9]. For example, Bressel et al. have proposed to estimate the health state of the PEM fuel cell using an observer-based prognostics algorithm and a state variable was created to track its degradation [10]. Wu et al. have predicted the stack voltage degradation of PEM fuel cells by developing a self-adaptive relevance vector machine, which is able to provide 20 hours ahead forecast time [11]. Both model-based and data-driven prognostics methods have been developed. For example, Pan et al. have proposed a model-based prognostics method based on Electrochemical Impedance Spectroscopy (EIS) measurement and an analytical equivalent circuit model, in which the parameters are obtained by linear regression [12]. A semi-empirical model-based prognostics method based on the adaptive unscented Kalman filter (AUKF) algorithm has been proposed in [13] to improve the initial parameters setting problem. Recent researches have seen increasing interests in developing

<sup>1</sup>Corresponding author. E-mail address: meiling.yue@femto-st.fr

1 data-driven prognostics methods, which can reflect the inherent  
2 relationships between the input and output by simulating  
3 neural networks and avoid the study of complicated physical  
4 mechanisms. Data-driven methods have gradually become the  
5 main methodology for fuel cell prognostics due to their easy-  
6 to-use and flexible modelling properties [14, 15, 16, 17]. For  
7 example, echo state network (ESN) has been deployed to fuel  
8 cell prognostics in recent works thanks to its improve compu-  
9 tation efficiency [18, 19, 20]. It was first applied to the predic-  
10 tion of the mean cell voltage of a degrading fuel cell in [21]  
11 where the accuracy and the computation time are studied re-  
12 garding the ESN parameters. Furthermore, for predicting the  
13 fuel cell health state, a multi-reservoir ESN has been devel-  
14 oped in [22] to optimize the parameterization process and in  
15 [23], an advanced structure of using moving weight matrix has  
16 been proposed to improve the prediction accuracy. However,  
17 these studies are limited to the stack level and have not fully  
18 considered variable and dynamic loads that may exist in most  
19 automotive applications. In those cases, the degradation of the  
20 PEM fuel cells cannot be easily quantified using the measured  
21 stack voltage, whose value is also affected by system operat-  
22 ing dynamics [24]. A degradation indicator reflecting intrinsic  
23 degradation level in dynamic operating conditions is required.  
24 Some researchers have proposed hybrid degradation indexes in  
25 multi-time scales for online operation, however, they are lim-  
26 ited to certain components and the accuracy is not satisfying  
27 [25]. Li et al. have proposed to represent the dynamic voltage  
28 response of the PEM fuel cell using linear parameter-varying  
29 models, and then obtained a real-time health indicator based on  
30 the online identified model [18]. However, the proposed health  
31 index in [18] only evaluates the overall performance loss and  
32 lacks the insights of fuel cell intrinsic degradation analysis. As  
33 the degradation of the fuel cell is related not only to the ageing  
34 phenomenon but also to the time-varying online operating con-  
35 ditions, developing a degradation identification method adapted  
36 to random external conditions is required.

37 This paper contributes to proposing an innovative degrada-  
38 tion identification method for the PEM fuel cell operating in  
39 real time, especially under dynamic load. A degradation indica-  
40 tor is proposed based on the fuel cell polarization model, which  
41 is extracted using a non-linear regression process regardless of  
42 the operation conditions. Following that, a multi-step window-  
43 sliding ESN prognostics method is applied to predict the future  
44 evolution of the degradation indicator which is identified on-  
45 line. The parameterization of the ESN is optimized by a ge-  
46 netic algorithm that ensures improved prediction performance.  
47 The proposed degradation identification and prognostics meth-  
48 ods are verified with a long-term operation experimental dataset  
49 of PEM fuel cell. ~~As there is no additional device to integrate~~  
50 ~~into the embedded fuel cell system, the prognostics can thus~~  
51 ~~be performed in real time.~~ As the measurements are obtained  
52 non-intrusively and the proposed method uses directly the out-  
53 put voltage signal, the prognostics can thus be performed in real  
54 time.

55 The main contributions of this paper can be summarized as  
56 follows:

1. A real-time degradation indicator of PEM fuel cells is  
proposed that can be extracted in both static and dy-  
namic/random operation conditions;
2. An enhanced multi-step ESN-based prognostics strategy is  
adapted for the prediction purpose;
3. The configuration of the proposed prognostics strategy is  
optimized through a genetic optimization algorithm.
4. The proposed prognostics strategy is validated by the long-  
term experimental PEM fuel cell degradation data.

The rest of the paper is organized as follows: Section 2  
describes the long-term fuel cell degradation experiment and  
the dataset used to validate the proposed method. Section 3  
explains the degradation identification method and Section 4  
presents the enhanced multi-step window-sliding ESN prognos-  
tics strategy. Finally, Section 5 concludes the paper.

## 2. Data description

A long-term fuel cell degradation experiment was carried  
out in FCLAB Research Federation<sup>2</sup>, France, and supported  
by the PRODIG project, which received funding from region  
Aquitaine, France. The test bench consists of a hydrogen tank,  
a pressure reducer, purge valves and hydrogen inlet valves, DC  
electric loads, DC power modules, two fuel cell stack mod-  
ules, a compact data acquisition system and a computer for con-  
trol and data logging. The structure of the two-fuel-cell-stack-  
module is shown in Figure 1. One of the stack modules is used  
for the dynamic load test, which is supposed to be applied in  
electric bicycles and is, therefore, tested using a dynamic load  
profile acquired in real operating conditions. The fuel cell stack  
is designed with an open cathode and dead-end anode structure  
and a 24 Vdc air fan is integrated with the stack for air supply  
and temperature regulation. The speed of the air fan is regu-  
lated by varying the duty cycle of an input PWM signal of 25  
kHz so that the temperature is controlled at the optimal level.  
Moreover, in the cathode side, the air is supplied with an air  
fan. With the air fan, sufficient quantity of air is guaranteed in  
normal operation. In other words, the fuel cells always work in  
the high stoichiometry mode. The pressure in the cathode side  
is kept equal to the atmosphere pressure. On the anode side, the  
pressure of hydrogen is fixed and a purge is performed every 30  
seconds. The fuel cells are self-humidified. Some critical pa-  
rameters of the studied fuel cell stack module are listed in Table  
1.

The dynamic load profile is obtained in real operating con-  
ditions of a hydrogen bike, which is supplied by a 36 V battery,  
while the fuel cell is used as a range extender, connected in par-  
allel with the battery. Both are used to supply the bike with an  
average power demand of 53.6 W. A 2.5-hour operation profile  
is shown in Figure 2, in which the fuel cell starts up to charge  
the battery until the battery's state-of-charge (SOC) gets to a  
pre-defined threshold and shuts down when the battery is fully  
charged. Based on this profile, the current load profile for the

<sup>2</sup>FCLAB Research Federation: <http://www.fc1ab.fr/>

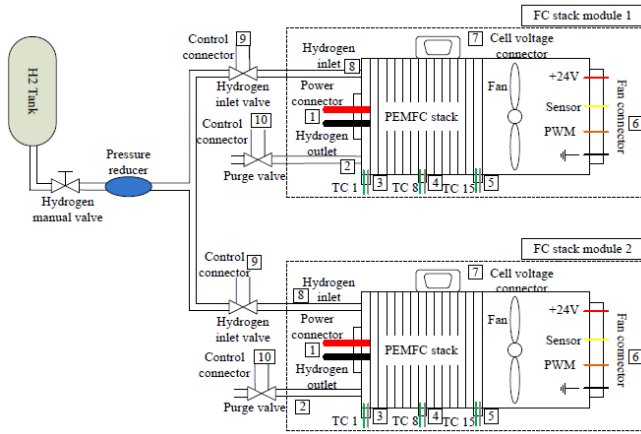


Figure 1: Two-fuel-cell-module structure

Table 1: Parameters of the studied fuel cell stack module

Parameter	Value
Active surface	33.625 cm <sup>2</sup>
Number of cells	15
Nominal pressure at hydrogen inlet	0.35 bar
Nominal output power	73.5 W
Maximum operating temperature	75 °C
Maximum current	13.45 A (0.4 A/cm <sup>2</sup> )
Lowest permitted stack voltage	7.5 V
Pressure interval at hydrogen inlet	0.1 to 0.4 bar

1 long-term PEM fuel cell degradation experiment is reproduced  
 2 to reach 1500 hours of operation time. The stack voltage and  
 3 the current are recorded with a sampling frequency of 5 Hz and  
 4 the characterization of the stack is performed every week by  
 5 collecting polarization curves.

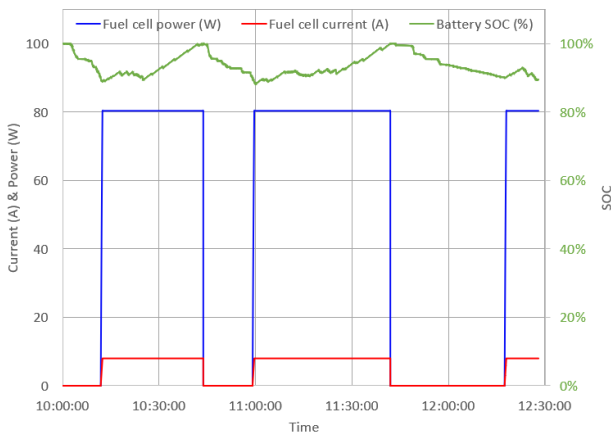


Figure 2: Test profile of a hydrogen bike

6 The measured stack voltage is shown in Figure 3. Some details  
 7 of the stack voltage and the corresponding current profile  
 8 are plotted in Figure 4 (a) and Figure 4 (b), respectively. Some  
 9 unintentional stops happen during the experiment due to test  
 10 bench incidents. As the degradation of the fuel cell is on a  
 11 longer time scale, i.e., thousands of hours, the stops have little

influence on its long-term performance loss.

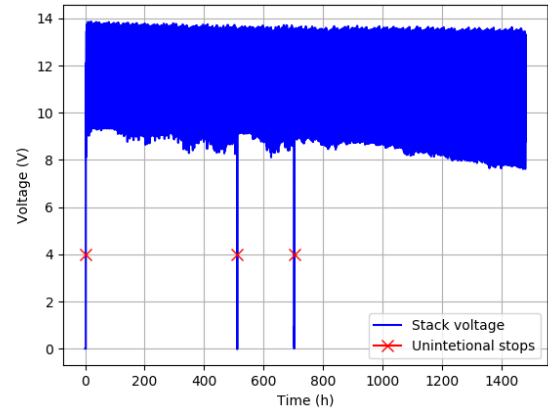
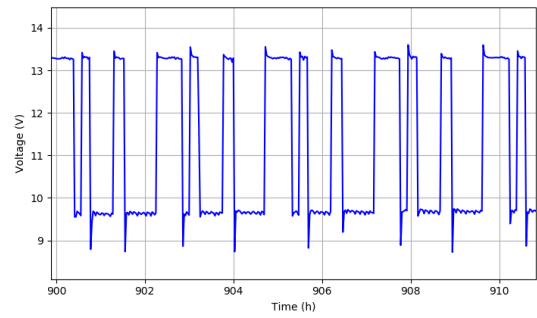
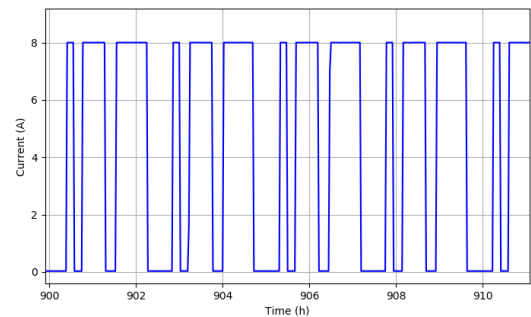


Figure 3: Stack voltage evolution in the dynamic operating test



(a) Details of the stack voltage evolution



(b) Details of the current profile

Figure 4: Details of the stack voltage and the corresponding current profile

### 3. Degradation Identification

The performance loss process of the PEM fuel cell stack shown in Figure 3 may be due to different causes, e.g., varying thermal and humidity state, fuel starvation, cycling with large voltage dynamics, etc. It is hard to represent its performance loss by the stack voltage evolution as it is also dependent on the load characteristics and system dynamics. Confronted with this problem, a **time-varying** degradation indicator is proposed

in this section to evaluate the degradation of the PEM fuel cell operating under such dynamic load.

### 3.1. Fuel cell polarization model

The polarization test is a common method to characterize a fuel cell. Polarization curve displays the stack voltage output  $V_{fc}$  against its operating current  $i$ . The polarization curve model of a  $n$ -cell fuel cell can be built as the reversible cell voltage  $V_0$  subtracting several irreversible losses including the activation losses and the crossover losses  $V_{act+cross}$ , the ohmic losses  $V_{ohmic}$ , the concentration losses  $V_{conc}$ :

$$V_{fc} = nV_{cell} = n(V_0 - V_{act+cross} - V_{ohmic} - V_{conc}) \quad (1)$$

A detailed parametric model of  $V_{cell}$  is derived in [26, 27]:

$$V_{cell}(i) = V_0 - \frac{RT}{2aF} \ln\left(\frac{i_{loss} + i}{i_0}\right) - iR_{eq} - B_c \ln\left(1 - \frac{i}{i_L}\right) \quad (2)$$

where  $R$  is the gas constant,  $T$  is the operating temperature,  $F$  is the Faraday constant,  $a$  is charge transfer coefficients of the electrodes,  $i_{loss}$  is the stack internal current, which is assumed to be assimilated to the hydrogen crossover current alone and there is no current caused by membrane shorting,  $i_0$  is the exchange current at the electrodes,  $R_{eq}$  is the equivalent ohmic resistance,  $B_c$  is an empirical parameter considering the water and gas accumulation effects and  $i_L$  is the limiting current at the cathode [27].

### 3.2. Degradation description

To find an adequate degradation indicator for the PEM fuel cell operating under dynamic current, it is important to know that which component degradation will cause which parameter varies in (2). Some parameters, like  $R$  and  $F$ , are constant.  $T$  is controlled in the experiment so that it is also regarded as constant, so as  $V_0$ . Some parameters are difficult to know whether they vary with time or not, therefore, they are set to fit the model with the measurements, namely  $a$  and  $B_c$ .  $i_{loss}$  is not considered as it is assumed to be assimilated to the hydrogen crossover current. Thus, the variations of the left three parameters,  $R_{eq}$ ,  $i_0$  and  $i_L$ , should be considered as the source of degradation.

$R_{eq}$ : The resistance increase can be caused by various phenomena. It includes the electronic and contact resistance increase, as well as the ionic resistance increase related to the membrane degradation [27]. The increase of the electronic and contact resistance can be observed at the surface layer of the bipolar plates, the electrode/electrolyte interface, etc, while the increase of the ionic resistance is dominant by the electrolyte materials and influenced by the membrane water concentration and temperature [28].

$i_0$ : The effective exchange current is a function of the electrode catalyst loading and the catalyst specific surface area [29]. For the fuel cell operated under dynamic load, the cycling will lead to the major degradation of the electrodes: the catalyst layer degradation and the carbon support degradation, especially, the catalyst loss is aggravated by the potential cycles [30].

$i_L$ : The limiting current on the cathode varies due to the changes on the diffusivity of oxygen, the gas pressure and the thickness of the gas diffusion layer [31]. The diffusivity and the pressure of the oxygen at the cathode are dominated cause of the concentration loss, which are influenced by the gas and water accumulation and can be recovered or mitigated by proper water management. The thickness of the gas diffusion layer cannot change over some nanometers, therefore, it can be ignored [27].

Some works have modelled the variation of the three parameters using physical models or semi-empirical models, however, some of them are developed with assumptions, which have not been validated [27]. Moreover, complex parameters bring difficulties when performing prognostics and some measurements needed in the model are not economically or technically feasible, therefore, establishing a degradation indicator that can track the degradation of the PEM fuel cell is necessary.

### 3.3. Degradation indicator $\alpha$

Figure 5 plots the polarization curves measured in the 2nd, 4th, 5th, 8th and 9th weeks, which indicates different degrees of fuel cell degradation. The polarization curves were obtained by varying the current value between 0 and the maximum (10 A). 8 current values, as shown in Figure 5, were set increasingly to the test stack through an electronic load. For each test point, the current value was maintained for 10 minutes to get a stable voltage measurement. Then the polarization curves were formed by interconnecting the 8 test points in current-voltage coordinate plane.

The model of (2) is identified with different values of  $R_{eq}$ ,  $i_0$  and  $i_L$ , whereas the evolutions of the parameters are shown in Figure 6. From Figure 6, it is found that the equivalent resistance  $R_{eq}$  increases by approximately 80%, while the exchange current  $i_0$  decreases by a rather same value. The fitting result of  $i_L$  has remained nearly constant. It is due to that under the dynamic cycling load, the water accumulation is well managed and contributes rarely to the concentration loss. This observation inspires us to assume the same linear evolution of  $R_{eq}$  and  $i_0$  and assign a constant value to  $i_L$ . Therefore, a unique time-varying variable  $\alpha(t)$  is chosen to describe the deviation of the parameters, which reflects the state of health of the fuel cell:

$$R_{eq} = R_{eq,init} \cdot (1 + \alpha(t)) \quad (3)$$

$$i_0 = i_{0,init} \cdot (1 - \alpha(t)) \quad (4)$$

The introduction of variable  $\alpha(t)$  ensures the identification of the fuel cell degradation level in the dynamic operation of the fuel cell. Even if the stack is operated under random load and the degradation cannot be directly identified by the voltage signal,  $\alpha(t)$  can be used as a degradation indicator to predict indicate the health state of the fuel cell.

As degradation can only be observed over long periods of at least several hundred hours, the fuel cell degradation is supposed to be quasi-constant on a short time scale, i.e., several hours [10, 32]. It allows us to segment the operation time into

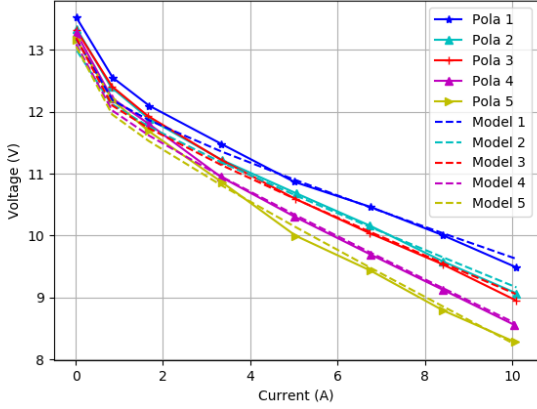


Figure 5: Polarization curves fitted with different  $\alpha$  values

1 short periods and fits the model with different  $\alpha$  values on each  
2 segment. This is realised by wrapping the pre-defined function  
3 as a model, which contains several parameters and an independ-  
4 ent variable  $\alpha$ , and fitting it using the Levenberg-Marquardt  
5 algorithm [33]. The pseudo-code is shown in Algorithm 1.

---

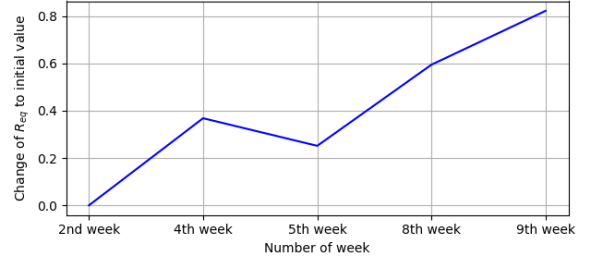
**Algorithm 1** Identification of the degradation indicator  $\alpha$

---

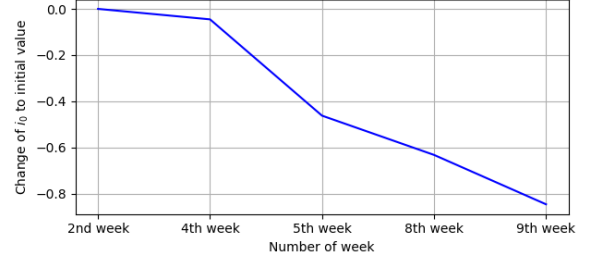
Load available measurement data of  $I, V$        $\triangleright$  Load data  
Initialize the parameters in model (2)       $\triangleright$  Initialization  
**Define:**  
Interval =  $l$   
Number of steps =  $j$   
Time step  $i = 0$   
**for**  $i = 0, \dots, j$ , **do**  
    Define model (2) with (3) and (4)       $\triangleright$  Model definition  
    Input  $X = I[0 + i * l : l + i * l]$        $\triangleright$  Segmentation  
    Output  $Y = V[0 + i * l : l + i * l]$   
    Fit the model with  $\alpha$  and find the best fit       $\triangleright$  Model fit  
**end for**

---

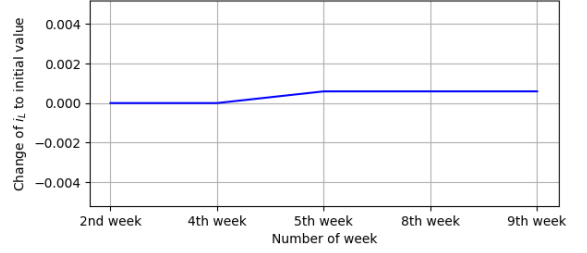
6 The identification result is shown in Figure 7 and the details  
7 are in Figure 8, in which the voltage measurement is segmented  
8 with an interval of 3 hours. It can be noticed that the voltage dy-  
9 namics in load transition periods are not well established using  
10 the identified degradation indicator and the polarization curve  
11 model. In fact, the voltage dynamics in transition states are  
12 mainly caused by system dynamics, such as thermal dynam-  
13 ics, which is not considered in the polarization curve model.  
14 The evolution of the extracted  $\alpha$  is shown in Figure 9, in which  
15 some recoveries in the signal are observed. These recoveries are  
16 reversible degradation phenomena due to the characterizations,  
17 which are of different operating conditions that affect the gas  
18 and water diffusion within the cells are affected. However, these  
19 reversible phenomena are part of transient regimes and will dis-  
20 appear once the stack comes back to a permanent regime. As  
21 the implementation of prognostics relies on the degradation in-  
22 formation contained in the signal, the extracted  $\alpha$  is smoothed  
23 using a Savitzky–Golay filter to avoid the influence of distur-



(a) Change of  $R_{eq}$  to its initial value



(b) Change of  $i_0$  to its initial value



(c) Change of  $i_L$  to its initial value

Figure 6: Evolution of degradation parameters  $R_{eq}$ ,  $i_0$  and  $i_L$

ing information.

## 4. ESN-based prognostics method

A data-driven prognostics method based on neural network  
modelling is proposed in this section. The idea is to use the  
available dataset to build the system behaviour model and to  
project the current system state to the future. Data-driven pro-  
gnostics methods have the model-free advantage that can be ap-  
plied regardless of the physical characteristics of the system. In  
this section, a typical recurrent neural network (RNN), i.e., the  
ESN, is adapted for the prognostics purpose.

### 4.1. Principle of ESN

The ESN has seen its wide use in time-series prediction ap-  
plications [34]. Different from traditional RNNs, the ESN uses  
a "reservoir pool" to build the structure of nonlinear systems,  
which achieves high prediction speed and competitive predic-  
tion performance. The implementation of the ESN is shown in  
Figure 10 and explained in what follows.

The state update model of ESN is written as:

$$\tilde{\mathbf{u}}(t) = f(\mathbf{w}_{res}\mathbf{u}(t-1) + \mathbf{w}_{in}\mathbf{x}(t)) \quad (5)$$

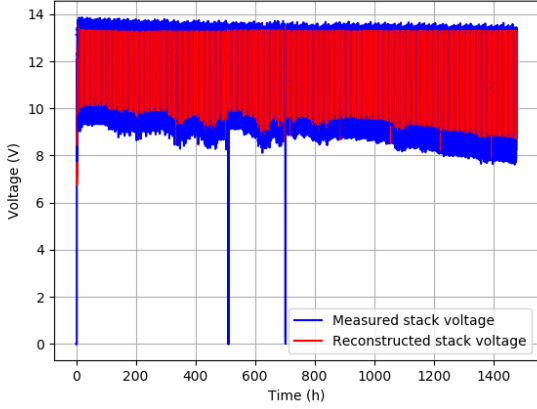


Figure 7: Reconstructed and measured stack voltages

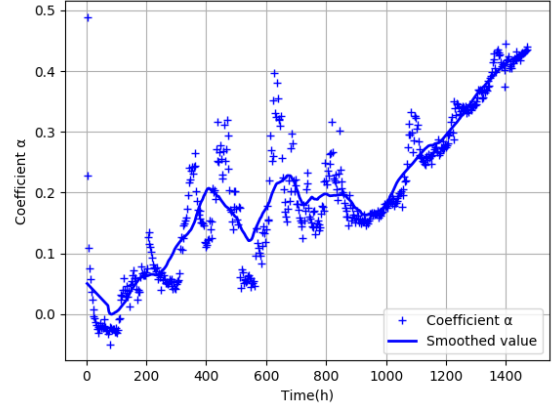


Figure 9: Evolution of the dynamic degradation indicator  $\alpha$

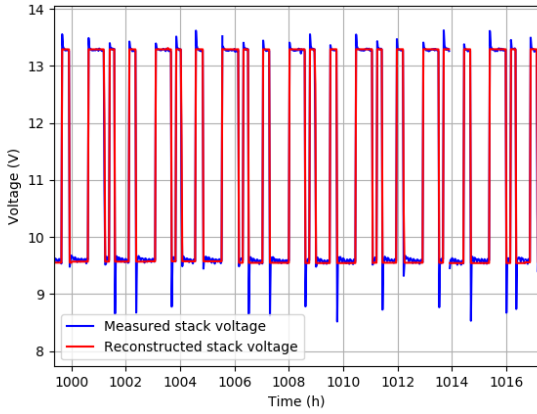


Figure 8: Details of the reconstructed and the measured stack voltages

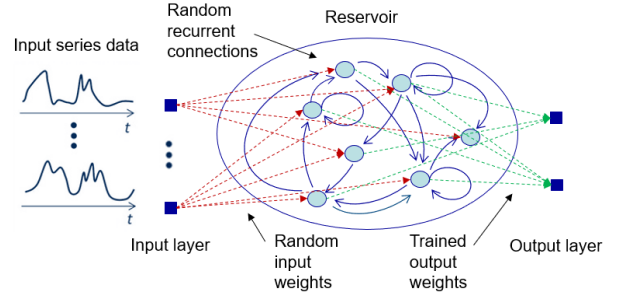


Figure 10: ESN structure illustration

culated according to (5) and (6). The output weight matrix is calculated as:

$$\mathbf{w}_{out} = (\Psi_t^T \Psi_t + \lambda \mathbf{I})^{-1} \Psi_t^T \mathbf{Y}_t \quad (8)$$

where  $\mathbf{I}$  is  $N_u$  order unit matrix,  $\lambda$  is the regulation parameter and

$$\Psi = [1; \mathbf{X}_t; \mathbf{U}_t] = \begin{bmatrix} 1 & 1 & \dots & 1 \\ \mathbf{x}(1) & \mathbf{x}(2) & \dots & \mathbf{x}(N_t) \\ \mathbf{u}(1) & \mathbf{u}(2) & \dots & \mathbf{u}(N_t) \end{bmatrix} \quad (9)$$

The general working procedure is as following:

1. Choose the size of the reservoir  $N_u$  and other parameters concerning the level of sparsity of connection, as well as the leakage;
2. Generate the input weights  $\mathbf{w}_{in}$  by sampling from a random binomial distribution;
3. Generate the reservoir weights  $\mathbf{w}_{res}$  by sampling from a uniform distribution;
4. Calculate the update of the state in the reservoir as the activation function  $f(\bullet)$  of the input at the current time step multiplied by the weights plus the previous state multiplied by the the reservoir weights, as written in (5);
5. Create input sequences and connect them to the desired outputs using linear regression and obtain the trained ESN.

1 where  $\mathbf{x}(t) \in \mathbb{R}^{N_x}$  and  $\mathbf{y}(t) \in \mathbb{R}^{N_y}$  are the input and output,  
2 which, in this study, are the sequences of the degradation indicator  $\alpha$ ,  $\mathbf{u}(t) \in \mathbb{R}^{N_u}$  is the internal state in the reservoir and  
3  $\tilde{\mathbf{u}}(t) \in \mathbb{R}^{N_u}$  is its update,  $\tilde{\mathbf{u}}(t) = \mathbf{u}(t) - \mathbf{u}(t-1)$ ,  $\mathbf{w}_{in} \in \mathbb{R}^{N_u \times (1+N_x)}$   
4 is the input weight matrix,  $\mathbf{w}_{res} \in \mathbb{R}^{N_u \times N_u}$  is the recurrent weight  
5 matrix in the reservoir, and  $\mathbf{w}_{out} \in \mathbb{R}^{N_y \times (1+N_x+N_u)}$  is the out-  
6 put weight matrix.  $k$  is the leaking rate with a range of (0, 1].  
7 The  $\tanh$  function is generally adopted as the activation function  
8  $f(\bullet)$  of the reservoir, and  $g(\bullet)$  of the output layer could  
9 be defined with a simple linear function such as  $g(\bullet) = 1$ .  $\mathbf{w}_{in}$   
10 and  $\mathbf{w}_{res}$  are initialized randomly and they are constant so that  
11 there is no need to train them. Only  $\mathbf{w}_{out}$  is going to be trained  
12 by linear regression. When the training dataset is provided, denoted  
13 as  $\mathbf{X}_t = [\mathbf{x}(1), \dots, \mathbf{x}(N_t)]$  and  $\mathbf{Y}_t = [\mathbf{y}(1), \dots, \mathbf{y}(N_t)]$ , where  
14  $N_t$  is the number of sequences in the input and the output, the  
15 corresponding reservoir states,  $\mathbf{U}_t = [\mathbf{u}(1), \dots, \mathbf{u}(N_t)]$  can be cal-

1 Based on the procedure of training an ESN, an input window  
2 and a prediction window need to be defined, which are used to  
3 formulate the input sequences and the output sequences of the  
4 ESN, respectively. The input window length is the length of the  
5 input sequence and the prediction window length is how many  
6 steps are going to be predicted following the input sequence.  
7 The input window length and the prediction window length are  
8 selected according to the volume of available input data. Sup-  
9 posing the number of available measurements  $s$  is up to  $N$ , a  
10 window length of  $p$  is used for the input sequence, written as:

$$\mathbf{x}(i) = [s(i+1), s(i+2), \dots, s(i+p)], \quad i = 0, \dots, N-p \quad (10)$$

11 For simplicity, it is written  $\mathbf{x}(i) = [s(i+1) : s(i+p)]$  in the fol-  
12 lowing text. Then, the corresponding output with a prediction  
13 window length of  $q$  is written as:

$$\mathbf{y}(i) = [\hat{s}(i+p+1), \hat{s}(i+p+2), \dots, \hat{s}(i+p+q)], \quad (11)$$

$$i = 0, \dots, N-p$$

14 Similarly, it is written with the form of  $\mathbf{y}(i) = [\hat{s}(i+p+1) :$   
15  $\hat{s}(i+p+q)]$  in the following text.

#### 16 4.2. Adapt ESN for prognostics purpose

17 The prognostics process can be summarized as a process of  
18 estimating a system's remaining useful life and the uncertain-  
19 ties. The international organization for standardization (ISO)  
20 committee has defined prognostics as [35]:

21 Standard ISO 13381 (2004). *The aim of prognostics is*  
22 *the "estimation of time to failure and risk for one or*  
23 *more existing and future failure modes".*

24 Therefore, to perform prognostics, we need to predict the  
25 system performance until the system failure. Based on the time  
26 series forecasting process described in Section 4.1, the last  $p$ -  
27 length sequence in the training phase is used to predict a se-  
28 quence with the length of  $q$ . Then, the prognostics starts, in  
29 which we cannot predict the subsequent states because the in-  
30 put sequences run out, the prediction cannot continue. As we  
31 need to continue to predict the time series until the end of life  
32 of the system, new input sequences should be formulated to  
33 successively move the input window. Thus, to retain the degra-  
34 dation tendency and to manage the prediction uncertainty, the  
35 predicted values of the last step with a sliding window of length  
36  $m$  are reinjected to the input sequence of the next step, as shown  
37 in Figure 11. Therefore, the last  $m$  values of the input sequence  
38 are indeed the predicted values. This process allows the contin-  
39 uous formulation of the input even without measurements so  
40 that the prognostics can be realised. This process is repeated  
41 until reaching the end-of-life (EOL) threshold, which, in this  
42 paper, is supposed to be **the value of 0.423, 97% of the maxi-**  
43 **mum degradation of the tested fuel cell regarding the length of**  
44 **the experiment. 1400 hours for the tested fuel cell.**

45 The pseudo-code of implementing ESN adapted for prognos-  
46 tics purpose is shown as Algorithm 2, where  $N_{train}$  is the num-  
47 ber of training steps equal to  $N-p$  and  $N_{predict}$  is the prediction  
48 steps until the system's EOL.

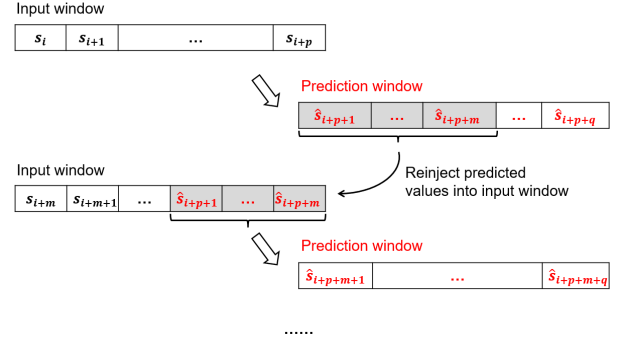


Figure 11: ESN adapted for prognostics purpose

#### 49 4.3. Implementation of ESN-based prognostics

50 In order to optimize the configuration of the ESN, the pro-  
51 posed ESN-based prognostics method consists of three phases:  
52 training phase, evaluation phase and prediction phase. The  
53 length of the identified degradation indicator  $\alpha$ , shown in Fig-  
54 ure 9, is also divided into three parts for the use of each phase.  
55 The ESN is trained in the training phase using the prepared in-  
56 put and output sequences and then, the following 400 hours are  
57 regarded as the evaluation phase. During the evaluation phase,  
58 the measurement is supposed to be unavailable so that the out-  
59 put sequence is reformulated by the predicted values of the last  
60 step. **The trained ESN model is used to output the predictions of**  
61  **$\alpha$  and the real values of  $\alpha$  is used to evaluate the performance of**  
62 **the prognostics. and determine optimal parameters of the ESN.**  
63 Here, the result of prognostics is evaluated by calculating the  
64 root mean square error (RMSE), written as (12). **In order to find**  
65 **the optimal settings of the ESN,** an optimization method, i.e.,  
66 the genetic algorithm (GA), is applied to **generate different pa-**  
67 **rameter combinations and run the prognostics algorithm repeat-**  
68 **edly until find the optimal settings. optimize the configuration**  
69 **of the ESN.** The idea is to code the unknown parameters into bi-  
70 nary digits, known as a chromosome, then, calculate the RMSE  
71 on the evaluation phase by selecting, crossover and mutating  
72 the chromosomes repeatedly until finding the optimal solution  
73 [36]. The advantage of GA is its ability to locate the global  
74 optimum or near-global optimum solution without exhausting  
75 search of the solution space. Besides, the processing time only  
76 increased as the square of the project size and not exponentially.  
77 Some configured parameters of the proposed ESN-based prog-  
78 nostics method and the adopted GA are listed in Table 2, where  
79 the length of the sliding window of  $m$  and the number of reser-  
80 voir **neurons**  $N$  are optimized by the GA. The influence of other  
81 ESN parameters in prognostics results is not so critical and the  
82 configuration method in [37] has been adopted.

$$RMSE = \sqrt{\frac{\sum_{k=1}^n (x_k - \hat{x}_k)^2}{n}} \quad (12)$$

83 Finally, in the prediction phase, no measurement is available  
84 while the ESN has already been optimized and validated by the  
85 evaluation phase, therefore, the data of both the training phase  
86 and the evaluation phase **are used to train the ESN and output**  
87 **the prognostics results on the prediction phase are entered into**

---

**Algorithm 2** ESN for prognostics purpose

```

Load training dataset  $s$                                 ▶ Load data
Smooth the training data                                ▶ Smoothing
Normalize the training data                            ▶ Normalization
Define:
Input window length =  $p$ 
Prediction window length =  $q$ 
Sliding window length =  $m$ 
Number of training steps =  $N_{train}$ 
Number of prediction steps =  $N_{predict}$ 
Time step  $i = 0$ 
while  $x_i < x_{EOL}$  do
  for  $i = 0, \dots, N_{train}$ , do                                ▶ Training phase
     $y_{train}[i, :] = s[i + p + 1 : i + p + q]$                 ▶ Prepare input
    and output
     $x_{train}[i, :] = s[i : i + p]$ 
  end for
  Fit the ESN with prepared input  $x_{train}$  and output  $y_{train}$ 
  Initialize  $x_{predict}[0, :]$  by connecting  $x[N_{train} + m : N_{train} +$ 
   $p]$  and  $y_{train}[-1, 0 : m]$ 
  for  $i = 0, \dots, N_{predict}$ , do                                ▶ Start prognostics
    Predict  $y_{predict}[i]$  using the fitted ESN and  $x_{predict}[i, :]$ 
    Reformulate  $x_{predict}[i, :]$  by connecting  $x_{predict}[i -$ 
     $1, m : p]$  and  $y_{predict}[i, 0 : m]$                                 ▶ Reformulate input
  end for
end while

```

---

Table 2: Configuration of ESN-based prognostics method

Parameter	Value
Input window length $p$	50
Prediction window length $q$	10
Leaking rate	0.2
Spectral radius	0.6
Regression parameter	0.01
GA population size	100
Number of generations	400
Length of chromosome	10

1 **the trained ESN model and output the prediction results.** The  
 2 whole procedure is shown in Figure 12. The prognostics results  
 3 are discussed in the following section.

#### 4.4. Result discussion

5 For comparison, at first,  $m$  is fixed at 1. The optimal  $N$  is  
 6 found between 10 and 400 using an iterating loop. The opti-  
 7 mal values of  $N$ , the RMSEs of the prognostics results in both  
 8 evaluation and prediction phases and the implementation time  
 9 with different training data lengths are recorded in Table 3. The  
 10 prognostics performance on the evaluation phase and the pre-  
 11 diction phase, as well as the errors are shown in Figure 13 for  
 12 a visual check. The beginning of the training phase has lower  
 13 accuracy because of the insufficient training data. After 200  
 14 hours, the training error is closed to zero, which demonstrates  
 15 that the configure ESN is of good performance. During the eval-  
 16 uation phase, the measurement is supposed to be unavailable so

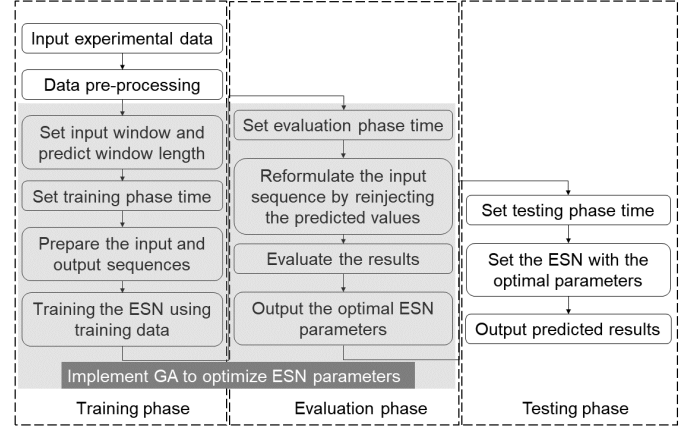


Figure 12: Procedure of ESN-based prognostics method

17 that the output sequence is reformulated by the predicted values  
 18 of the last step, as described in Section 4.2. The optimal result  
 19 is plotted in red dashed line. However, when it comes to the  
 20 prediction phase, the RMSEs get worse. This is because there  
 21 is only one predicted value being considered in the next step,  
 22 which could be accidental and cannot transfer enough informa-  
 23 tion. Moreover, the implementation time of GA is less than 1  
 24 minute, while the implementation time of ESN-based prognos-  
 25 tics is less than 1 second.

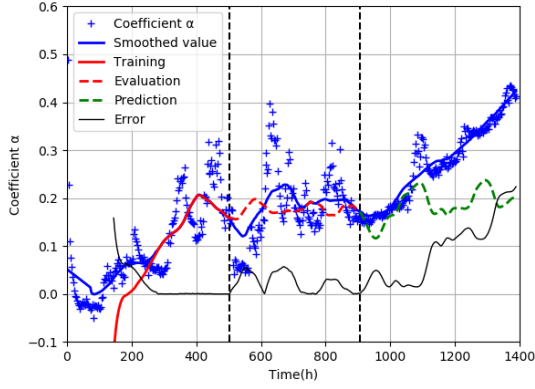
 Table 3: ESN-based prognostics results ( $m=1$ )

Training data length (hours)	500	600	700	800
$m$	1	1	1	1
$N$	90	94	83	81
RMSE of training	0.036	0.019	0.012	0.017
RMSE of evaluation	0.030	0.032	0.056	0.039
RMSE of prediction	0.112	0.140	0.304	0.182
Prognostics implementation time	0.93s	0.94s	0.93s	0.94s

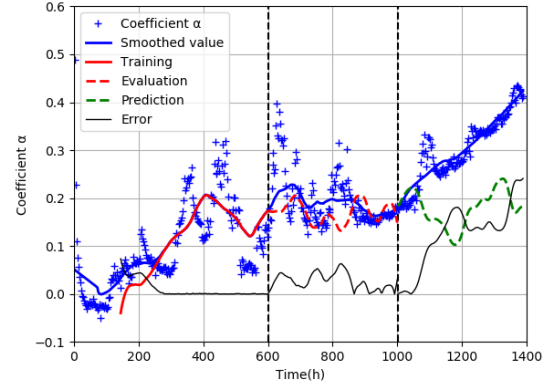
26 Figure 14 shows the prognostics results with different train-  
 27 ing data lengths, in which both  $m$  and  $N$  are optimized. The  
 28 GA optimization results of the two parameters and the RMSEs  
 29 of both the evaluation phase and the prediction phase, together  
 30 with the improvements compared with Table 3 are shown in Table 4.  
 31 By optimizing the number of values that are reinjected  
 32 into the input sequence of the next step, prognostics results in  
 33 the prediction phase have been improved up to 90.8%.

#### 4.5. Comparison with different methods

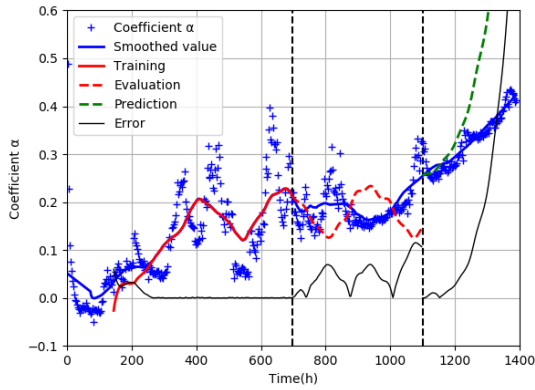
35 The proposed prognostics method is compared with differ-  
 36 ent methods in the literature. The comparison methods include  
 37 particle filter [9] and stacked long short-term memory (LSTM)  
 38 [38]. The training phase considers the same generated sam-  
 39 ples. In the compared particle filter method, a second order  
 40 exponential model is used, and the details of model parameters  
 41 of particle filter prognostics method is listed in Table 5. The  
 42 stacked LSTM used for comparison is with two hidden layers



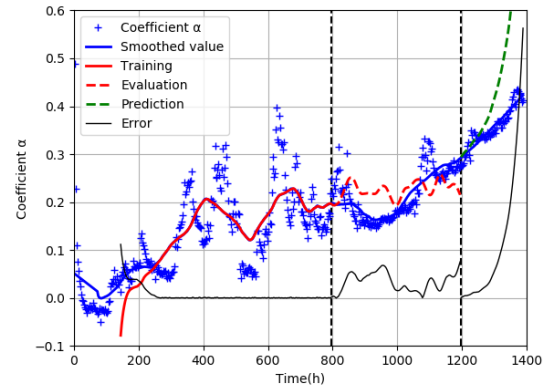
(a) Prediction result with training data length = 500 hours



(b) Prediction result with training data length = 600 hours



(c) Prediction result with training data length = 700 hours



(d) Prediction result with training data length = 800 hours

Figure 13: Implementation of prognostics with different training data lengths (optimizing  $N$ )

Table 4: GA optimization and ESN-based prognostics results (optimizing  $m$ )

Training data length (hours)	500	600	700	800
Optimized $m$	3	5	3	3
Optimized $N$	95	80	234	265
RMSE of training	0.017	0.019	0.019	0.005
RMSE of evaluation	0.031	0.039	0.047	0.033
Improvements of evaluation	-3.3%	2.5%	16.1%	1.5%
RMSE of prediction	0.051	0.017	0.028	0.020
Improvements of prediction	54.5%	87.9%	90.8%	89.0%
Prognostics implementation time	0.91s	0.90s	1.12s	1.03s

Table 5: Model parameters of particle filter prognostics method

Parameter	Value
Input dimension	1
Output dimension	1
Number of state variables	7
Number of particles	2000

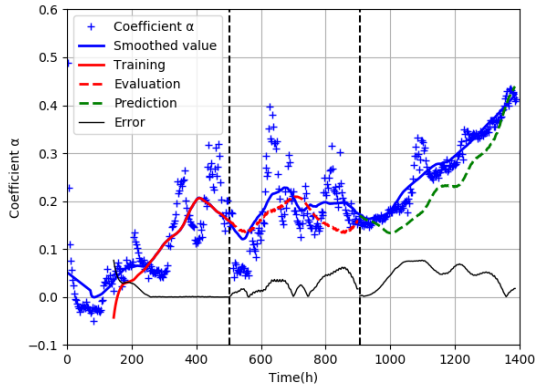
diction accuracy. Besides, the performance of stacked LSTM prognostics method is the worst due to the non-optimized configurations. When comparing the implementation time, the proposed ESN runs the fastest, which is more competitive for on-line applications.

## 5. Conclusion

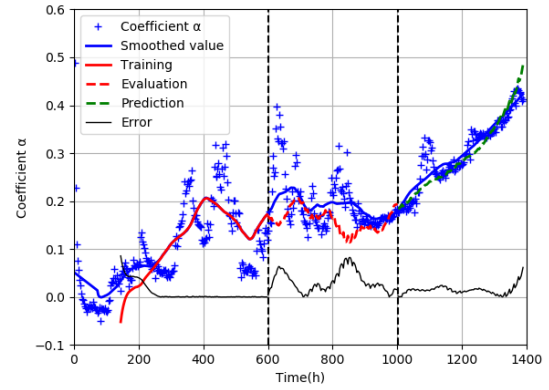
A degradation identification and prognostics method for real-time operating PEM fuel cells was proposed in this paper. The degradation indicator was derived based on the polarization model and could be extracted from the stack voltage measurements with random system dynamics. To perform prognostics, an enhanced multi-step ESN was adapted for the prediction purpose and the parameters of the ESN were optimized through an

and a dense (output) layer for prediction. The details of the configuration of the stacked LSTM prognostics method is shown in Table 6.

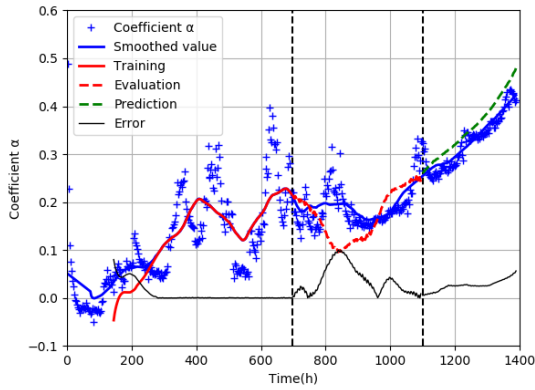
The performance of the three different prognostics method is compared in Table 7. As it can be seen from Table 7, the proposed multi-step ESN-based prognostics method has achieved the best prediction accuracy at 600-hour, 700-hour and 800-hour training data length, while the accuracy is worse than the particle filter method at 500-hour training data length. This is because when more information is fed to the model, the model can leverage more trend information, thus improving the pre-



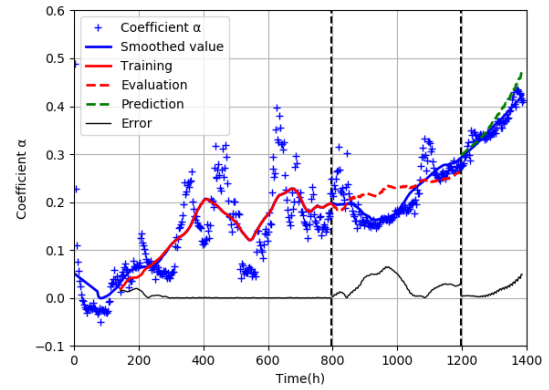
(a) Prediction result with training data length = 500 hours



(b) Prediction result with training data length = 600 hours



(c) Prediction result with training data length = 700 hours



(d) Prediction result with training data length = 800 hours

Figure 14: Implementation of prognostics with different training data lengths (optimizing  $m$  and  $N$ )

Table 6: Model parameters of stacked LSTM prognostics method

Parameter	Value
Time steps	4
Number of neurons on hidden layer 1	100
Number of neurons on hidden layer 2	100
Number of neurons on dense layer	1
Optimizer	adam
Loss	mean squared error
Epoch number	50
Batch size	50
Dropout rate	0.01

1 evaluation phase by a genetic algorithm. Compared to non-  
 2 optimized case, the RMSEs of the predictions were improved  
 3 up to 90.8% by introducing an optimized sliding window length  
 4 when reformulating the input of the ESN in the prognostics  
 5 phase. Moreover, the proposed method achieved better accu-  
 6 racy and less computation time when comparing with other  
 7 prognostics methods.

8 The proposed method of degradation identification and progn-  
 9 nostics allows one to estimate and predict the PEM fuel cell  
 10 health state under variable and dynamic operating conditions.  
 11 The degradation identification can be realized in real time with-

12 out using supplementary measurements and the prognostics  
 13 strategy is model-free. This method is control-oriented and can  
 14 facilitate the development of degradation tolerant control strate-  
 15 gies as well as advanced predictive maintenance solutions.

## Acknowledgment

16 This paper is supported by the project HAEOLUS, funded  
 17 by the Fuel Cells and Hydrogen 2 Joint Undertaking under the  
 18 European Union's Horizon 2020 research and innovation pro-  
 19 gram under grant agreement No 779469. Any contents herein  
 20 reflect solely the authors' view. The FCH 2 JU and the Euro-  
 21 pean Commission are not responsible for any use that may be  
 22 made of the information herein contained. This work is also  
 23 supported by the EIPHI Graduate School (contract ANR-17-  
 24 EURE-0002) and the project PRODIG (1494C0045) funded by  
 25 French Environment and Energy Management Agency.  
 26

## References

- 27  
 28 [1] S. Kong, M. Bressel, M. Hilaret, R. Roche, Advanced passivity-  
 29 based, aging-tolerant control for a fuel cell/super-capacitor hy-  
 30 brid system, *Control Engineering Practice* 105 (2020) 104636.  
 31 doi:<https://doi.org/10.1016/j.conengprac.2020.104636>.

Table 7: Comparison of prognostics methods

Training data length (hour)	500		600		700		800	
	RMSE	Time	RMSE	Time	RMSE	Time	RMSE	Time
Partile filter [9]	0.042	4.19s	0.035	4.45s	0.049	4.73s	0.047	5.25s
Stacked LSTM [38]	0.079	6.81s	0.078	7.31s	0.078	7.11s	0.051	7.47s
Proposed ESN	0.051	0.91s	0.017	0.90s	0.028	1.12s	0.020	1.03s

- [2] J. M. Kurtz, H. N. Dinh, Fuel cell technology status: Degradation, Tech. rep., National Renewable Energy Lab.(NREL), Golden, CO (United States) (2018).
- [3] R. Keller, S. Ding, M. Müller, D. Stolten, Fault-tolerant model predictive control of a direct methanol-fuel cell system with actuator faults, *Control Engineering Practice* 66 (2017) 99 – 115. doi:https://doi.org/10.1016/j.conengprac.2017.06.008.
- [4] J. Luna, E. Usai, A. Husar, M. Serra, Enhancing the efficiency and lifetime of a proton exchange membrane fuel cell using nonlinear model-predictive control with nonlinear observation, *IEEE Transactions on Industrial Electronics* 64 (8) (2017) 6649–6659. doi:10.1109/TIE.2017.2682787.
- [5] G. Wang, F. Huang, Y. Yu, S. Wen, Z. Tu, Degradation behavior of a proton exchange membrane fuel cell stack under dynamic cycles between idling and rated condition, *International Journal of Hydrogen Energy* 43 (9) (2018) 4471 – 4481. doi:https://doi.org/10.1016/j.ijhydene.2018.01.020.
- [6] J. Han, J. Han, S. Yu, Experimental analysis of performance degradation of 3-cell pemfc stack under dynamic load cycle, *International Journal of Hydrogen Energy* 45 (23) (2020) 13045 – 13054. doi:https://doi.org/10.1016/j.ijhydene.2020.02.215.
- [7] P. Ren, P. Pei, Y. Li, Z. Wu, D. Chen, S. Huang, Degradation mechanisms of proton exchange membrane fuel cell under typical automotive operating conditions, *Progress in Energy and Combustion Science* 80 (2020) 100859. doi:https://doi.org/10.1016/j.peccs.2020.100859.
- [8] R. Ma, T. Yang, E. Breaz, Z. Li, P. Briois, F. Gao, Data-driven proton exchange membrane fuel cell degradation predication through deep learning method, *Applied Energy* 231 (2018) 102 – 115. doi:https://doi.org/10.1016/j.apenergy.2018.09.111.
- [9] M. Jouin, R. Gouriveau, D. Hissel, M.-C. Péra, N. Zerhouni, Prognostics of pem fuel cell in a particle filtering framework, *International Journal of Hydrogen Energy* 39 (1) (2014) 481 – 494. doi:https://doi.org/10.1016/j.ijhydene.2013.10.054.
- [10] M. Bressel, M. Hilairet, D. Hissel, B. Ould Bouamama, Remaining useful life prediction and uncertainty quantification of proton exchange membrane fuel cell under variable load, *IEEE Transactions on Industrial Electronics* 63 (4) (2016) 2569–2577. doi:10.1109/TIE.2016.2519328.
- [11] Y. Wu, E. Breaz, F. Gao, D. Paire, A. Miraoui, Nonlinear performance degradation prediction of proton exchange membrane fuel cells using relevance vector machine, *IEEE Transactions on Energy Conversion* 31 (4) (2016) 1570–1582. doi:10.1109/TEC.2016.2582531.
- [12] R. Pan, D. Yang, Y. Wang, Z. Chen, Health degradation assessment of proton exchange membrane fuel cell based on an analytical equivalent circuit model, *Energy* 207 (2020) 118185. doi:https://doi.org/10.1016/j.energy.2020.118185.
- [13] H. Liu, J. Chen, C. Zhu, H. Su, M. Hou, Prognostics of proton exchange membrane fuel cells using a model-based method, *IFAC-PapersOnLine* 50 (1) (2017) 4757 – 4762, 20th IFAC World Congress. doi:https://doi.org/10.1016/j.ifacol.2017.08.947.
- [14] H. Liu, J. Chen, D. Hissel, H. Su, Short-term prognostics of pem fuel cells: A comparative and improvement study, *IEEE Transactions on Industrial Electronics* 66 (8) (2019) 6077–6086. doi:10.1109/TIE.2018.2873105.
- [15] R. Ma, Z. Li, E. Breaz, C. Liu, H. Bai, P. Briois, F. Gao, Data-driven prognostics of proton exchange membrane fuel cell degradation, *IEEE Transactions on Industry Applications* 55 (4) (2019) 4321–4331. doi:10.1109/TIA.2019.2911846.
- [16] D. Zhou, A. Al-Durra, K. Zhang, A. Ravey, F. Gao, A robust prognostic indicator for renewable energy technologies: A novel error correction grey prediction model, *IEEE Transactions on Industrial Electronics* 66 (12) (2019) 9312–9325. doi:10.1109/TIE.2019.2893867.
- [17] J. Ma, X. Liu, X. Zou, M. Yue, P. Shang, L. Kang, S. Jemei, C. Lu, Y. Ding, N. Zerhouni, Y. Cheng, Degradation prognosis for proton exchange membrane fuel cell based on hybrid transfer learning and intercell differences, *ISA Transactions* (2020). doi:https://doi.org/10.1016/j.isatra.2020.06.005.
- [18] Z. Li, Z. Zheng, R. Outbib, Adaptive prognostic of fuel cells by implementing ensemble echo state networks in time-varying model space, *IEEE Transactions on Industrial Electronics* 67 (1) (2020) 379–389. doi:https://doi.org/10.1109/TIE.2019.2911846.
- [19] S. Morando, S. Jemei, D. Hissel, R. Gouriveau, N. Zerhouni, Proton exchange membrane fuel cell ageing forecasting algorithm based on echo state network, *International Journal of Hydrogen Energy* 42 (2) (2017) 1472–1480. doi:https://doi.org/10.1016/j.ijhydene.2016.05.286.
- [20] Z. Hua, Z. Zheng, M.-C. Péra, F. Gao, Remaining useful life prediction of pemfc systems based on the multi-input echo state network, *Applied Energy* 265 (2020) 114791. doi:https://doi.org/10.1016/j.apenergy.2020.114791.
- [21] S. Morando, S. Jemei, R. Gouriveau, N. Zerhouni, D. Hissel, Fuel cells prognostics using echo state network, in: *IECON 2013 - 39th Annual Conference of the IEEE Industrial Electronics Society, 2013*, pp. 1632–1637. doi:10.1109/IECON.2013.6699377.
- [22] R. Mezzi, S. Morando, N. Y. Steiner, M. C. Péra, D. Hissel, L. Larger, Multi-reservoir echo state network for proton exchange membrane fuel cell remaining useful life prediction, in: *IECON 2018 - 44th Annual Conference of the IEEE Industrial Electronics Society, 2018*, pp. 1872–1877. doi:10.1109/IECON.2018.8591345.
- [23] Z. Hua, Z. Zheng, M. C. Péra, F. Gao, Data-driven prognostics for pemfc systems by different echo state network prediction structures, in: *2020 IEEE Transportation Electrification Conference Expo (ITEC), 2020*, pp. 495–500. doi:10.1109/ITEC48692.2020.9161581.
- [24] Z. Li, S. Jemei, R. Gouriveau, D. Hissel, N. Zerhouni, Remaining useful life estimation for pemfc in dynamic operating conditions, in: *2016 IEEE Vehicle Power and Propulsion Conference (VPPC), 2016*, pp. 1–6. doi:10.1109/VPPC.2016.7791762.
- [25] H. Liu, J. Chen, D. Hissel, J. Lu, M. Hou, Z. Shao, Prognostics methods and degradation indexes of proton exchange membrane fuel cells: A review, *Renewable and Sustainable Energy Reviews* 123 (2020) 109721. doi:https://doi.org/10.1016/j.rser.2020.109721.
- [26] O. Z. Sharaf, M. F. Orhan, An overview of fuel cell technology: Fundamentals and applications, *Renewable and Sustainable Energy Reviews* 32 (2014) 810–853. doi:https://doi.org/10.1016/j.rser.2014.01.012.
- [27] M. Jouin, R. Gouriveau, D. Hissel, M.-C. Marion-Péra, N. Zerhouni, Degradations analysis and aging modeling for health assessment and prognostics of pemfc, *Reliability Engineering and System Safety* 148 (2016) 78 – 95. doi:https://doi.org/10.1016/j.res.2015.12.003.
- [28] A. Husar, S. Strahl, J. Riera, Experimental characterization methodology for the identification of voltage losses of pemfc: Applied to an open cathode stack, *International Journal of Hydrogen Energy* 37 (8) (2012) 7309–7315, iII Iberian Symposium on Hydrogen, Fuel Cells and Advanced Batteries, HYCELTEC-2011. doi:https://doi.org/10.1016/j.ijhydene.2011.11.130.
- [29] F. Barbir, Chapter five - fuel cell operating conditions, in: F. Barbir (Ed.), *PEM Fuel Cells (Second Edition)*, second edition Edition, Academic Press, Boston, 2013, pp. 119–157. doi:https://doi.org/10.1016/B978-0-12-387710-9.00005-9.
- [30] S. S. Khan, H. Shareef, M. Kandidayeni, L. Boulon, A. Amine, E. H. Abdennebi, Dynamic semiempirical pemfc model for prognostics and fault diagnosis, *IEEE Access* 9 (2021) 10217–10227. doi:10.1109/ACCESS.2021.3049528.
- [31] J. M. Morgan, R. Datta, Understanding the gas diffusion layer in proton exchange membrane fuel cells. i. how its structural characteristics affect diffusion and performance, *Journal of Power Sources* 251 (2014) 269–

- 1 278. doi:<https://doi.org/10.1016/j.jpowsour.2013.09.090>.
- 2 [32] M. Jouin, M. Bressel, S. Morando, R. Gouriveau, D. Hissel, M.-C. Péra,  
3 N. Zerhouni, S. Jemei, M. Hilairat, B. Ould Bouamama, Estimating the  
4 end-of-life of pem fuel cells: Guidelines and metrics, *Applied Energy* 177  
5 (2016) 87 – 97. doi:<https://doi.org/10.1016/j.apenergy.2016.05.076>.
- 6 [33] J. J. Moré, The levenberg-marquardt algorithm: Implementation and theory,  
7 in: G. A. Watson (Ed.), *Numerical Analysis*, Springer Berlin Heidelberg,  
8 Berlin, Heidelberg, 1978, pp. 105–116.
- 9 [34] H. Jaeger, The "echo state" approach to analysing and training recurrent  
10 neural networks, GMD Report 148, GMD - German National Research  
11 Institute for Computer Science (2001).
- 12 [35] ISO13381-1, Condition monitoring and diagnostics of machines e prog-  
13 nostics e part1: general guidelines, International Organization for Stan-  
14 dardization (2004).
- 15 [36] A. Chipperfield, P. Fleming, C. M. Fonseca, Genetic algorithm tools  
16 for control systems engineering, *Proceedings of Adaptive Computing  
17 in Engineering Design and Control* 23 (01 1994). doi:10.1016/S1474-  
18 6670(17)49015-X.
- 19 [37] M. Lukoševičius, *A Practical Guide to Applying Echo State Networks*,  
20 Springer Berlin Heidelberg, Berlin, Heidelberg, 2012, pp. 659–686.  
21 doi:10.1007/978-3-642-35289-8-36.
- 22 [38] F.-K. Wang, X.-B. Cheng, K.-C. Hsiao, Stacked long short-  
23 term memory model for proton exchange membrane fuel cell sys-  
24 tems degradation, *Journal of Power Sources* 448 (2020) 227591.  
25 doi:<https://doi.org/10.1016/j.jpowsour.2019.227591>.